Mon. Not. R. Astron. Soc. **339,** 669–679 (2003)

Parsec-scale Faraday rotation distribution in the BL Lac object 1803+784

D. C. Gabuzda[1,2★†] and V. A. Chernetskii[3]

[1]*Joint Institute for VLBI in Europe, Postbus 2, 7990 AA Dwingeloo, the Netherlands*
[2]*Astro Space Centre, Lebedev Physical Institute, 53 Leninskii Pr., 117924 Moscow, Russia*
[3]*Sternberg Astronomical Institute, 13 Universitetskii pr., 119899 Moscow, Russia*

Accepted 2002 October 22. Received 2002 September 9; in original form 2001 November 14

ABSTRACT

We present the results of VLBI polarization observations of the BL Lac object 1803+784 made simultaneously at 22, 15, 8 and 5 GHz in 1997 April, and quasi-simultaneously at 1.6 and 5 GHz in 1998 July. These data have yielded the total intensity, polarization, spectral-index, and rotation-measure distributions on scales from less than 1 mas to about 30 mas from the core (from a projected distance of about 1–150 pc at the redshift of 1803+784). There is an enhancement in the rotation measure for the VLBI core, clearly due to plasma in the immediate vicinity of the AGN. The rotation measures 10–30 mas from the core demonstrate that the Galactic contribution to the total observed rotation measures is equal to the previously reported integrated rotation measure (-61 rad m^{-2}). After subtracting this Galactic contribution and multiplying by $(1+z)^2$, the rotation measure for the VLBI core in the source rest frame is about 500 rad m^{-2}, similar to the VLBI core rotation measures reported previously for BL Lac and several quasars.

Key words: polarization – radio continuum: galaxies.

1 INTRODUCTION

BL Lacertae objects are compact, flat-spectrum active galactic nuclei with weak, sometimes undetectable, optical line emission and strong variability in total intensity and linear polarization over a broad range of wavelengths from γ-ray/X-ray to radio. It is believed that synchrotron radiation is the dominant emission mechanism virtually throughout the spectrum. The origin of the relative low luminosity of their optical line emission is not clear.

The BL Lac object 1803+784 has a redshift $z = 0.68$ (Lawrence et al. 1987). The dominant orientation of the inner $\sim$10 mas of the VLBI jet is nearly directly west (Witzel et al. 1988; Gabuzda et al. 1992); further from the core, the jet begins to curve to the south (Britzen et al. 1999), toward the arcsec-scale structure (Strom & Biermann 1991; Kollgaard et al. 1992). Evidence for motion on smaller scales that is not colinear with the dominant east–west structure has been found in VLBI studies at higher frequencies (e.g. Krichbaum et al. 1993) or with polarization sensitivity (Gabuzda et al. 1994; Gabuzda & Cawthorne 1996). The total intensity structure shows a remarkably persistent stationary feature roughly 1.5 mas west of the core, which has been detectable in VLBI images for more than two decades (Schalinski et al. 1988; Witzel et al. 1988). Based on analyses of centimetre-wavelength VLBI polarization images, it was initially proposed that this feature was associated with a transverse shock.

Space VLBI (VSOP; Hirabayashi et al. 1998) total intensity (I) and linear polarization (P) images at 5 GHz revealed an appreciably curved inner jet structure within $\sim$1–2 mas of the core, with the observed polarization electric vectors everywhere aligned with the local jet direction. If the observed polarization vectors have not been significantly affected by Faraday rotation or relativistic aberration effects, this indicates that the magnetic ($\boldsymbol{B}$) field is transverse all along the inner jet (Gabuzda 1999). There is no evidence for substantial Faraday rotation along the line of sight to the 5-GHz VLBI jet (Gabuzda 2000, confirmed by our results below), and, given the good alignment of the polarization vectors with the local jet direction, it is unlikely that they are subject to appreciable aberration effects. Thus, it is likely that, indeed, the $\boldsymbol{B}$ field is transverse along this part of the VLBI jet. The shock mechanism for generating transverse $\boldsymbol{B}$ fields would require that we are seeing a whole series of shocks along the curved VLBI jet, each of which enhances the local transverse field. An alternative that may provide a more natural interpretation of the observed polarization structure is that the transverse $\boldsymbol{B}$ fields represent the toroidal component of a helical $\boldsymbol{B}$ field associated with the jet, or alternatively correspond to the toroidal field associated with the current along the jet (e.g. Istomin & Pariev 1994; Blandford 2003).

A comparison of a 1.6-GHz VSOP space-VLBI P image with a 5-GHz ground-array P image made from data acquired just one day later provided tentative evidence for inhomogeneity in the rotation-measure distribution in this part of the jet, with the core and

★E-mail: gabuzda@phys.ucc.ie
†Present address: Physics Department, University College Cork, Cork, Ireland.

stationary jet feature nominally having modest but different rotation measures (Gabuzda 2000). However, it was difficult to know whether this result could be trusted, since the comparison was based on measurements at only two widely-spaced frequencies.

We present here VLBA *I* and *P* images of 1803+784 at 22, 15, 8, and 5 GHz constructed from data obtained simultaneously at these four frequencies in 1997 April, as well as VLBI images obtained at 5 and 1.6 GHz in 1998 July. We concentrate here on the results for the 1997 April images, and present only a partial analysis of the 1998 July images, which will be considered in more detail in a future paper.

We were able to determine the spectrum of the core and several individual features in the VLBI jet. The jet components display a wide range of spectra, from inverted to optically thin power-laws. The four-frequency polarization images clearly show an enhancement of the rotation measure in the vicinity of the VLBI core. Estimates of the associated thermal electron density and line-of-sight magnetic field suggest values fairly typical of narrow-line clouds. 'De-rotation' of the observed polarization vectors based on the derived rotation-measure distribution demonstrates that the jet ***B*** field is transverse to the jet on all scales out to about 30 mas from the VLBI core, consistent with the idea that we are detecting the dominant toroidal component of a helical field.

We adopt throughout the values for the cosmological constants $H_o = 75$ km s^{-1} Mpc^{-1} and $q_o = 0.5$.

2 OBSERVATIONS AND REDUCTION

2.1 1997 April

1803+784 was one of six compact BL Lac objects observed with the VLBA with polarization sensitivity on 1997 April 6, simultaneously at 22, 15, 8 and 5 GHz. Eight baseband converters (BBCs) of 8 MHz each were used, with four recording right-circular polarization and four left-circular polarization. Two-bit sampling was used, with a total data rate of 64 Mbits s^{-1} per polarization (VLBA mode 128-4-2). A summary of the frequencies observing in each BBC at each frequency are summarized in Table 1. The *u*–*v* coverage obtained for the 5-GHz data for 1803+784 are shown in Fig. 1; the coverage at the other frequencies is essentially identical but scaled accordingly.

The data reduction and imaging were done in the AIPS package using standard techniques (see chapter 9 in the AIPS 'Cookbook', available at www.nrao.edu). The amplitudes were calibrated using system temperatures measured during the observing run and the known gain curves of the VLBA antennas. The initial calibration of the phases was performed using narrow-band phase-calibration tones injected into the data stream during the observations. This procedure removed the phase offsets between the BBCs for all four correlations. The residual frequency-dependent phase variations (delays) and their time dependence (the delay rates) were then solved for using the AIPS task FRING.

The instrumental polarizations ('D-terms') were derived from the fully self-calibrated data for the unpolarized source 3C 84 using the AIPS task LPCAL. This assumes that the D-terms enter the *RL* and *LR* correlations in a linear fashion and that their magnitude does not exceed ∼10 per cent, which are very good assumptions for the VLBA antennas. We also assumed that 3C 84 was unpolarized, which is a very good assumption at 5, 8 and 15 GHz, where 3C 84 is completely depolarized. This assumption is slightly violated at 22 GHz, where there is weak but detectable polarization in the jet of 3C 84 far from the VLBI core, however, this small amount of polarization is not sufficient to significantly affect the overall solutions for the D-terms. This may contribute to a higher 'noise' level in the 22-GHz polarization maps, but does not significantly affect the properties of reliably detected polarization in the target sources.

Table 1. Observing frequencies (GHz).

BBC	5 GHz	8 GHz	15 GHz	22 GHz
1	4.97149	8.40549	15.34949	22.21749
2	4.97949	8.41349	15.35749	22.22549
3	4.98749	8.42149	15.36549	22.23349
4	4.99549	8.42949	15.37349	22.24149

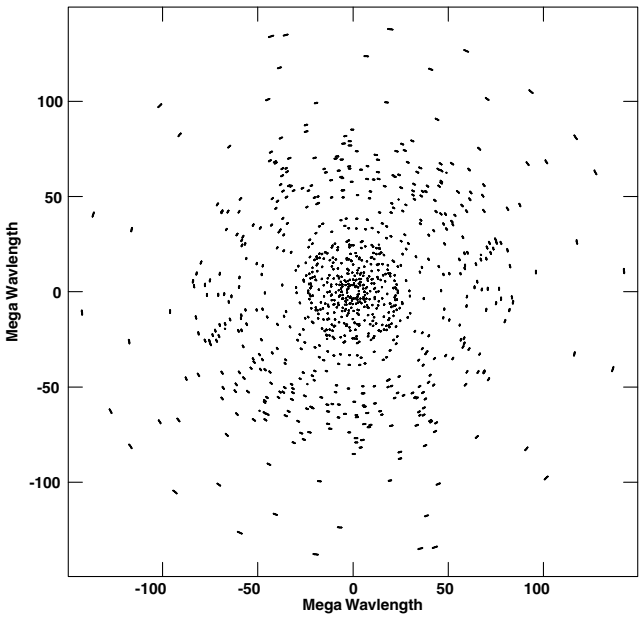

Figure 1. Baseline (*u*–*v*) coverage for 1997 April VLBA observations of 1803+784 at 5 GHz. The horizontal (*u*) axis is reversed from its usual definition.

The absolute orientation of the polarization electric vector position angle (EVPA) was calibrated using VLA observations obtained over about two hours on 1997 April 6, simultaneous with the VLBA observations. The primary EVPA calibrators for the VLA observations were 3C 138 and 3C 48, for which we assumed that twice the polarization angles were $2\chi = -24^\circ$ and -145°, respectively. The VLBI polarization angles χ were calibrated by assuming that, for a source with sufficiently compact polarization, the true χ for the total VLBI polarization should coincide with the measured χ for the VLA core at the observing epoch. The compact polarized source used for this purpose was BL Lac, for which more than 90 per cent of the integrated polarized flux was detected on mas scales.

2.2 1998 July

Space VLBI observations of 1803+784 were obtained at 1.6 GHz on 1998 July 20, and at 5 GHz on 1998 July 21, as part of the VSOP project (Hirabayashi et al. 1998). In both cases, the orbiting antenna and the VLBA were used; in addition, the 1.6-GHz ground array included the phased VLA and the 70-m Goldstone antenna, and the 5-GHz ground array included the 100-m Effelsberg antenna. Partial results for the full-resolution space-VLBI observations have been presented by Gabuzda (1999, 2000), and a more detailed analysis

will be presented in a future paper; we consider here only the 1.6- and 5-GHz images made using the ground VLB arrays alone, focusing on the detection of polarized emission 10–30 mas from the core.

The data reduction and imaging were done in the AIPS package using standard techniques. The resulting u–v coverage was similar to that in Fig. 1, but with more continuous tracks and scaled accordingly.

The D-terms were derived from observations of 1803+784 using the AIPS task LPCAL, solving simultaneously for the D-terms and the source polarization. The groups of CLEAN components used to represent individual polarized regions in the source were selected by hand. The absolute orientation of the polarization electric vectors was calibrated as indicated above using integrated measurements from VLA observations obtained at both 1.6 and 5 GHz on 1998 July 20. The primary polarization-angle calibrator for the VLA observations was 3C286, for which we assumed twice the polarization angle to be 66°. The compact polarized source used for this purpose was 1803+784 itself, for which about 80 per cent of the integrated polarized flux was detected on mas scales.

3 RESULTS FOR 1997 APRIL

Figs 2–5 show contour images of the total and linearly polarized flux density for each of the four frequencies observed in 1997 April. The superposed sticks show the orientation of the polarization position angles χ. The beam sizes are indicated by ellipses in the bottom left-hand corner of each image.

We obtained circular Gaussian model fits to the I and P visibility data at each frequency using the model-fitting software in the Brandeis VLBI package (Roberts, Wardle & Brown 1994) as described by Gabuzda, Wardle & Roberts (1989). These models were based on the division into individual components suggested by an initial inspection of the CLEAN components and by the images themselves. The resulting models are listed in Table 2, which gives (column 1) the component designation (C = core, I = inner, S = stationary, O = outer), (columns 2–3) total flux I and its error, (columns 4–5) polarized flux p and its error, (columns 6–7) polarization position angle χ and its error, (column 8) degree of polarization m, (column 9) distance from the core r, (column 10) structural position angle relative to the core θ, (column 11) size of the circular Gaussian representing the component. In the case of component S, the fits at 8, 15 and 22 GHz were substantially improved by fitting it as an elliptical Gaussian; for this component at these frequencies, columns (11)–(13) give the major axis, minor axis, and position angle of this elliptical component, which are very similar at all three frequencies.

The indicated errors are formal 1σ errors corresponding to an increase of χ^2 by unity. It is likely that these appreciably underestimate the true errors in some cases; in particular, since the formal errors for r and θ were unreasonably small in nearly all cases, we have not included them in Table 2.

The absolute errors on I and p are difficult to estimate, and will depend to some extent on the accuracy of the a priori amplitude calibration. The a priori calibration of the VLBA antennas at 5–15 GHz is better than 5 per cent, and the overall uncertainty introduced by uncertainties in the a priori calibration will be a factor of a few smaller than this, since the various amplitude uncertainties add incoherently. The accuracy will be somewhat worse at 22 GHz, where the amplitudes begin to be subject to atmospheric opacity affects. The errors in p yielded by the model fitting generally exceed those expected from incomplete subtraction of the D-terms (Roberts et al. 1994), suggesting they are reasonable estimates of the real over-

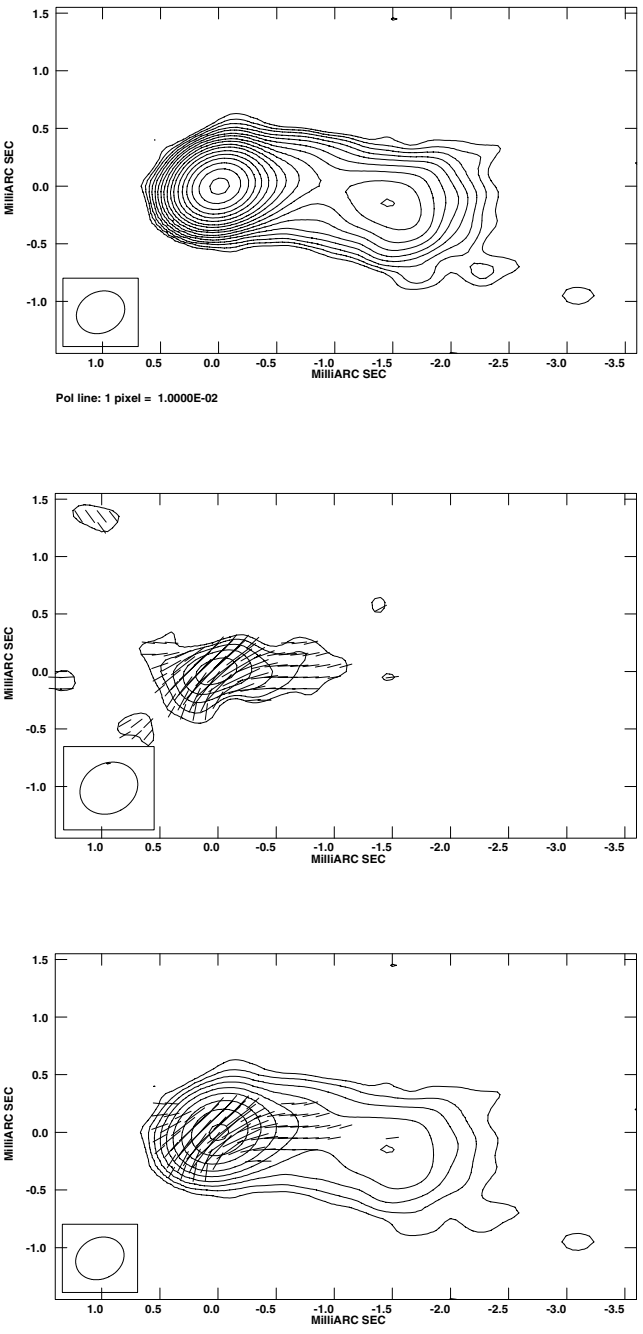

Figure 2. VLBI maps of 1803+784 at 22 GHz for 1997 April: (a) I, with contours at −0.35, 0.35, 0.5, 0.7, 1, 1.4, 2, 2.8, 4, 5.6, 8, 11, 16, 23, 32, 45, 64 and 90 per cent of the peak brightness of 1.272 Jy beam^{-1}. (b) P, with contours of polarized intensity at 20, 28, 40, 56, and 80 per cent of the peak brightness of 53.0 mJy beam^{-1}, and χ vectors superimposed. (c) The I image from (a) with every other contour omitted and χ sticks superimposed. The restoring beam is shown by the ellipse in the lower left-hand corner of each panel.

all errors in p. We estimated the upper limit to the polarization of feature S at 22 GHz using the noise level on the P image.

We will be most interested here in deriving adequate estimates of the errors in χ. The χ errors in Table 2 appear quite plausible. In fact, these errors are larger than the errors in χ expected from incomplete subtraction of the polarization D-terms (Roberts et al. 1994), suggesting that these uncertainties are reasonable estimates

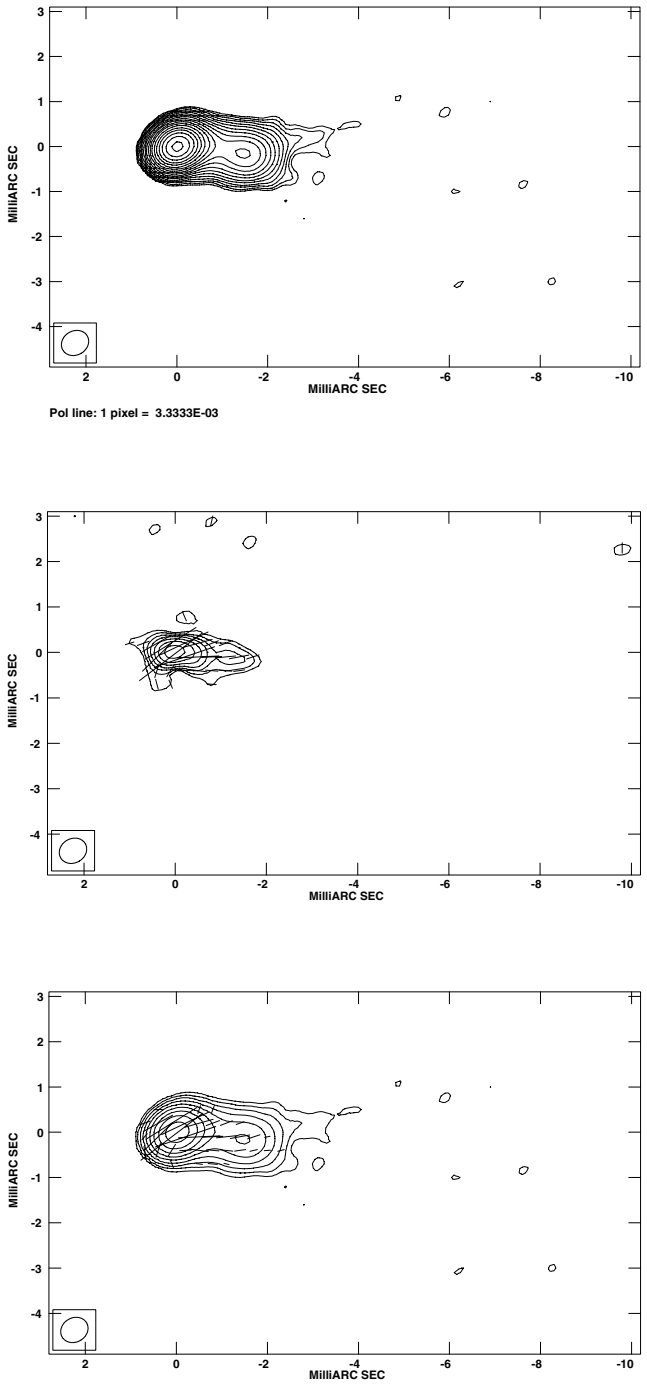

Figure 3. VLBI maps of 1803+784 at 15 GHz for 1997 April: (a) I, with contours at -0.25, 0.25, 0.35, 0.5, 0.7, 1, 1.4, 2, 2.8, 4, 5.6, 8, 11, 16, 23, 32, 45, 64 and 90 per cent of the peak brightness of 1.333 Jy beam^{-1}. (b) P, with contours of polarized intensity at 10, 14, 20, 28, 40, 56, and 80 per cent of the peak brightness of 49.4 mJy beam^{-1}, and χ vectors superimposed. (c) The I image from (a) with every other contour omitted and χ sticks superimposed. The restoring beam is shown by the ellipse in the lower left-hand corner of each panel.

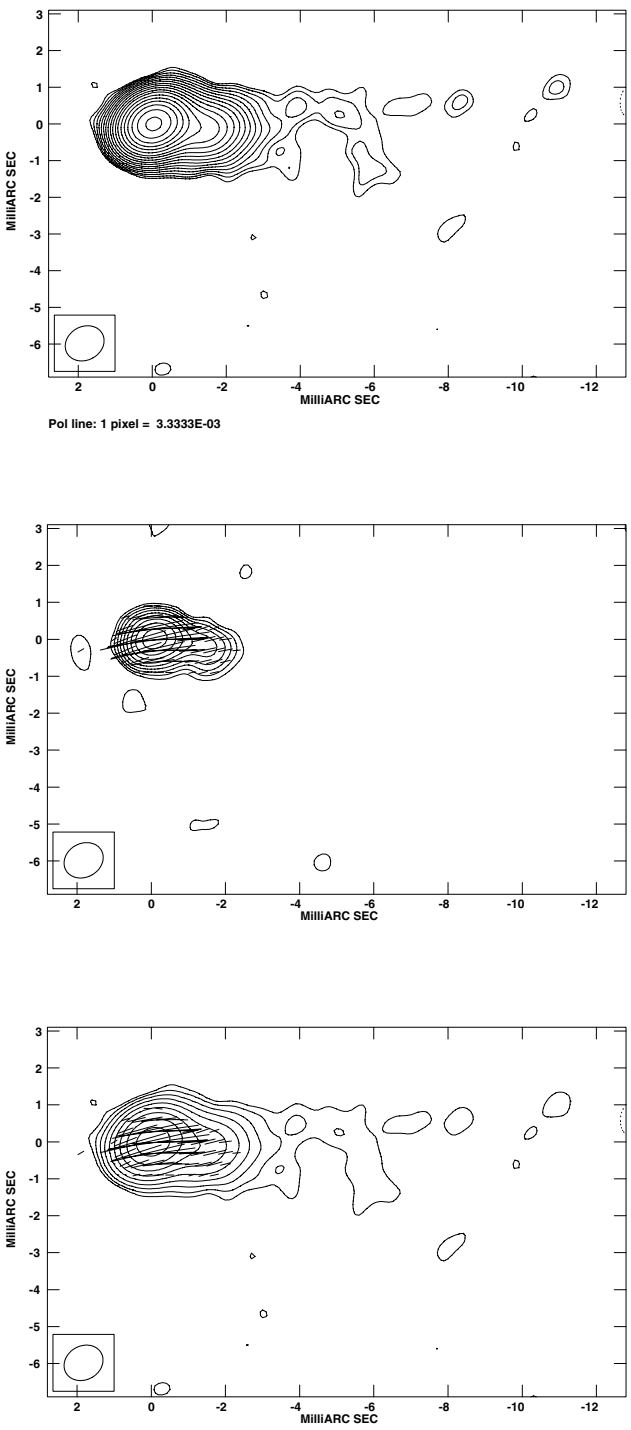

Figure 4. VLBI maps of 1803+784 at 8 GHz for 1997 April: (a) I, with contours at -0.25, 0.25, 0.35, 0.5, 0.7, 1, 1.4, 2, 2.8, 4, 5.6, 8, 11, 16, 23, 32, 45, 64 and 90 per cent of the peak brightness of 1.423 Jy beam^{-1}. (b) P, with contours of polarized intensity at 5, 7, 10, 14, 20, 28, 40, 56, and 80 per cent of the peak brightness of 47.0 mJy beam^{-1}, and χ vectors superimposed. (c) The I image from (a) with every other contour omitted and χ sticks superimposed. The restoring beam is shown by the ellipse in the lower left-hand corner of each panel.

of the errors in χ associated with the model fitting. There is also uncertainty introduced by the procedure described above for setting the VLBI EVPAs using integrated values obtained with the VLA. The simultaneity of the VLA and VLBA observations and the compactness of the polarizations of BL Lac (1997 April) and 1803+784 (1998 July) ensures that the uncertainty in this contribution to the absolute EVPA calibration is no more than 2–3°, as is also indicated by a comparison of the EVPA calibration results for other VLBA observations nearby in time using the same reference

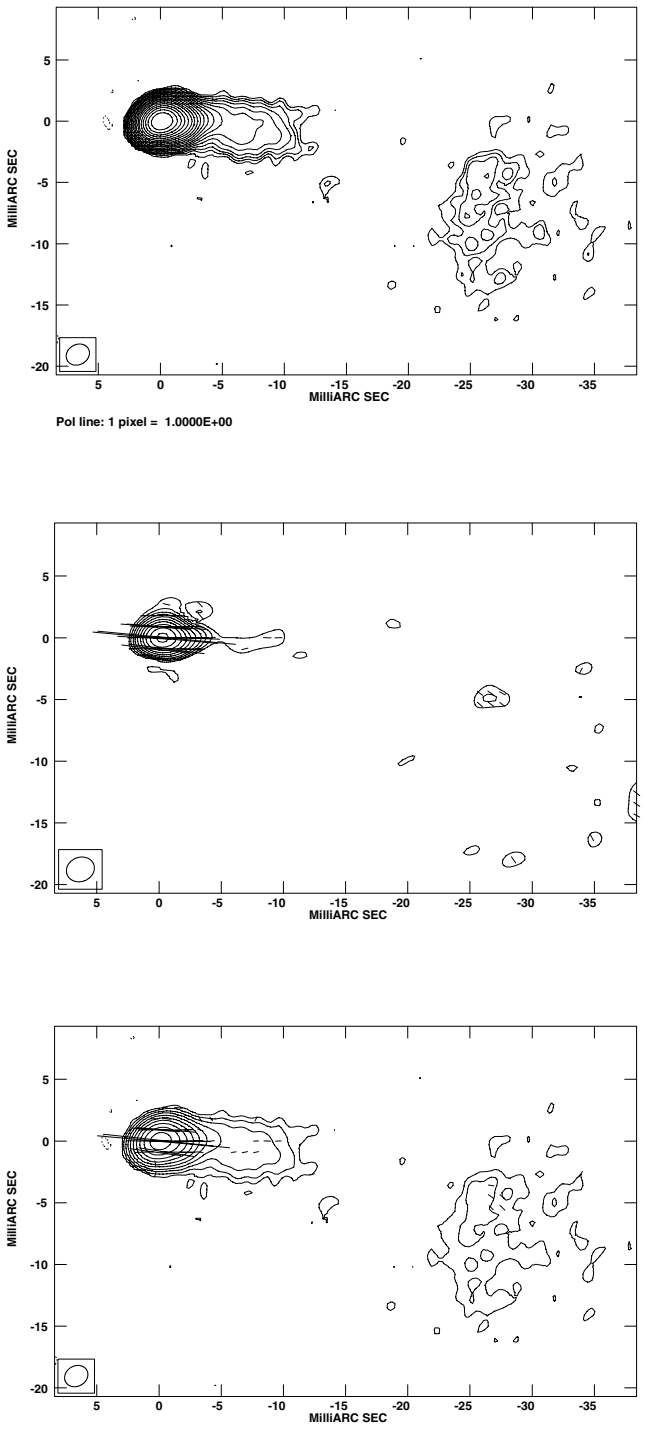

Figure 5. VLBI maps of 1803+784 at 5 GHz for 1997 April: (a) I, with contours at −0.12, 0.12, 0.18, 0.25, 0.35, 0.5, 0.7, 1, 1.4, 2, 2.8, 4, 5.6, 8, 11, 16, 23, 32, 45, 64 and 90 per cent of the peak brightness of 1.634 Jy beam^{-1}. (b) P, with contours of polarized intensity at 4, 5.6, 8, 11, 16, 23, 32, 45, 64, and 90 per cent of the peak brightness of 64.5 mJy beam^{-1}, and χ vectors superimposed. (c) The I image from (a) with every other contour omitted and χ sticks superimposed. The restoring beam is shown by the ellipse in the lower left-hand corner of each panel.

antenna, Los Alamos (see Reynolds, Cawthorne & Gabuzda 2001). The formal uncertainties that arise from the model fitting range from about 1°–10°. Therefore, the errors in Table 2 adequately reflect the real overall errors in χ in most cases; when the errors quoted in the table are less than 3°, the real errors are probably 3°–4°.

3.1 Spectral indices for individual components

Inspection of Table 2 shows that the structures on scales between the core and component S detected at the four frequencies agree very well. The components C, I1 and S are detected at all four frequencies, while I2 is not detected only at 5 GHz, where it is blended with the core. Accordingly, we can derive the spectra of each of these four components, presented in Fig. 6. The spectral indices between pairs of neighbouring frequencies are summarized in Table 3.

We can see that the core (triangles in Fig. 6) has a very flat spectrum at least from 8 to 22 GHz; it seems likely that it remains flat to 5 GHz, and that the higher flux at 5 GHz is due to blending with component I2.

The innermost knot I2 (circles in Fig. 6) at a distance of about 0.25 mas from the core was clearly detected only at 22, 15 and 8 GHz. The flux density measurements for these three frequencies suggest that the spectrum peaks near 15 GHz. I2 was not directly detected at 5 GHz, since it is blended with the core. However, we can make an educated guess about its 5-GHz flux by assuming that the core spectrum remains flat to 5-GHz and subtracting the 5-GHz core flux expected in this case ($\simeq$1196 mJy) from the total observed 5-GHz flux for the core blended with I2 (1314 mJy); this yields the hollow triangle for the core and the hollow circle for I2 in Fig. 6. This estimated 5-GHz flux density for I2 smoothly continues the trend shown by the other three frequencies, supporting the possibility that this component is either optically thick or appreciably absorbed below 15 GHz.

The component I1 (diamonds in Fig. 6) at a distance of about 0.6 mas from the core was detected at all four frequencies. It has a roughly power-law, optically thin spectrum between 5 and 15 GHz, which appears to flatten between 15 and 22 GHz. This behaviour is perhaps somewhat puzzling, but it does not appear to be due to errors associated with the 15 and 22-GHz fluxes, since the 22-GHz flux density from the model fit ($\sim$100 mJy) is substantially above the value corresponding to an extrapolation of the behaviour at the lower frequencies ($\simeq$70 mJy using the 15-GHz flux density and α_{8-15}, or as little as $\sim$20 mJy using the 8-GHz flux density and α_{5-8}). In addition, although the spectrum remains optically thin between 8 and 15 GHz, it is already showing signs of becoming less steep.

The long-lived, quasi-stationary jet component S has a nearly flat spectrum, consistent with a power-law with spectral index $\alpha = -0.11$ ($S \propto \nu^{\alpha}$).

3.2 Wavelength dependence of the polarization angles

An inspection of the four polarization images immediately makes it clear that the core polarization position angle is not constant with frequency. In addition, the rotation between 22 GHz and 5 GHz predicted by the *integrated* rotation measure (−61 rad m^{-2}; Wrobel 1993; Pushkarev 2001) is only about 12°, whereas a visual inspection of the 5 and 22 GHz polarization images suggests χ offset in the core closer to 45°.

If this frequency dependence of χ is due to external Faraday rotation, χ should vary linearly with λ^2, where λ is the observing wavelength, with the slope corresponding to the rotation measure. We present a plot of the observed χ values from our model fitting for the four well-isolated features detected at at least three frequencies as functions of λ^2 in Fig. 7. The χ values for the core, I1, and S obey λ^2 laws to within the errors: least-squares fit lines pass through the

Table 2. Source models.

	I (mJy)	ΔI (mJy)	p (mJy)	Δp (mJy)	χ (deg)	$\Delta\chi$ (deg)	m (per cent)	r (mas)	θ (deg)	MAJ (mas)	MIN (mas)	PA (deg)
						5 GHz						
C	1314	3	44.3	1.7	−90.6	1.1	3.4	–	–	0.05		
I1	381	3	19.0	1.3	−117.5	2.3	5.0	0.65	−89.0	0.44		
S	301	2	17.2	1.4	−78.9	3.0	5.7	1.60	−96.3	0.54		
O3	52	2	5.3	1.6	−101.1	7.1	10.2	3.24	−90.9	1.46		
O2	70	2	3.9	1.6	−85.0	8.7	5.6	7.28	−95.6	3.53		
O1	81	3	3.6	1.6	−119	11	4.4	27.58	−104.8	9.50		
						8 GHz						
C	1198	6	34.0	1.2	−57.8	1.0	2.8	–	–	0.00		
I2	183	7	29.9	1.2	−104.1	1.2	16.3	0.24	−87.9	0.26		
I1	135	6	6.1	1.3	−106.3	5.0	4.5	0.54	−83.7	0.41		
S	291	8	9.9	1.3	−73.9	3.0	3.4	1.47	−95.8	0.94	0.52	82
						15 GHz						
C	1197	3	43.6	2.4	−48.1	3.0	3.6	–	–	0.06		
I2	250	2	24.0	3.0	−91.4	3.0	9.6	0.26	−84.9	0.23		
I1	90	2	6.3	3.1	−95.5	10.7	7.0	0.66	−85.2	0.34		
S	252	3	10.3	2.8	−76.1	6.2	4.1	1.50	−96.1	0.80	0.47	81
						22 GHz						
C	1194	3	42.8	2.7	−42.0	2.0	3.6	–	–	0.05		
I2	216	3	13.5	3.4	−101.6	6.1	6.2	0.22	−86.9	0.18		
I1	101	2	7.8	3.4	−96.0	10.7	7.7	0.59	−84.8	0.35		
S	257	3						1.46	−96.2	0.88	0.49	77

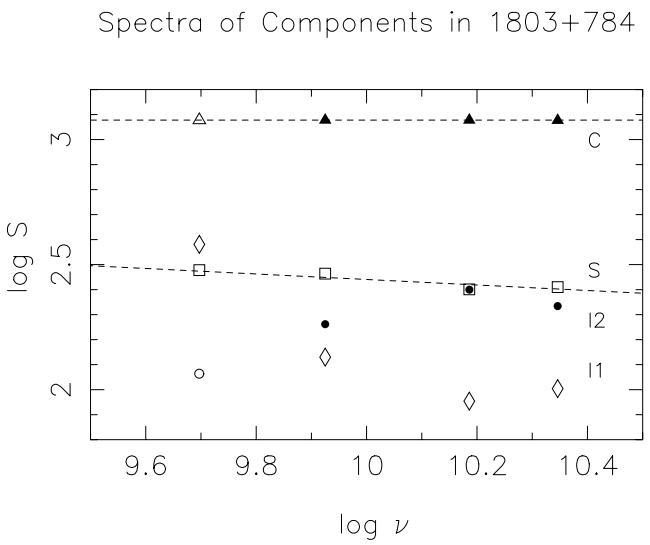

Figure 6. Spectra of the individual VLBI components C (the core, triangles), I2 ($r \simeq 0.25$ mas, circles), I1 ($r \simeq 0.6$ mas, diamonds), and S (quasi-stationary feature at $r \simeq 1.5$ mas, squares). All flux density estimates except the hollow triangle and circle at 5 GHz are taken directly from the model fitting; for an explanation of how these two estimates were derived, see the text.

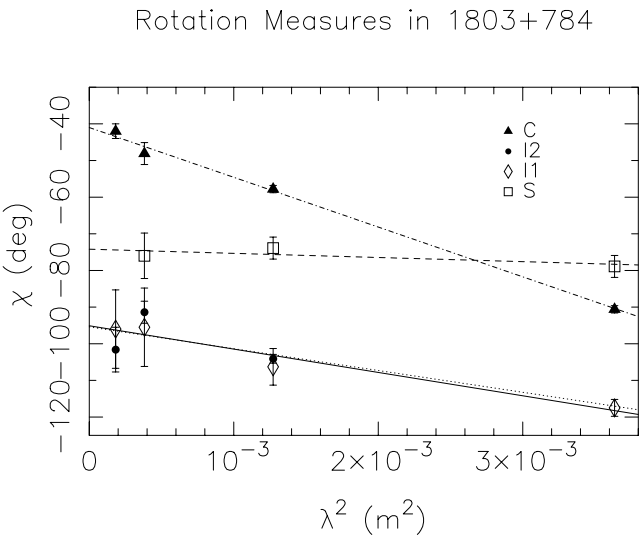

Figure 7. Polarization position angles χ as functions of the square of the observed wavelength λ^2 for C (the core, triangles and dot-dashed line), I2 ($r \simeq 0.25$ mas, circles and dotted line), I1 ($r \simeq 0.6$ mas, diamonds and solid line), and S ($r \simeq 1.5$ mas, squares and dashed line) for 1997 April. The χ errors shown are 1σ. The lines are least-squares linear fits to the measurements for each component.

Table 3. Component spectral indices ($S \propto \nu^{\alpha}$).

	Approximate r (mas)	α_{5-8}	α_{8-15}	α_{15-22}
C	–	–	+0.00	+0.01
I2	0.25	(+0.87)	+0.52	−0.40
I1	0.60	−1.98	−0.67	+0.31
S	1.50	−0.06	−0.24	+0.05

error bars of all points at the 1σ level. Thus, the observed χ values appear to manifest the influence of Faraday rotation. There is a gradient in the observed rotation measure from the core (RM $= -237 \pm 6$ rad m^{-2}) to I1 ($r \simeq 0.6$ mas, RM $= -111 \pm 13$ rad m^{-2}), and further to S ($r \simeq 1.5$ mas, RM $= -20 \pm 15$ rad m^{-2}).

The situation with I2 is not so clear. The conclusions concerning the rotation measure for this component are potentially complicated by several factors: (i) it was not detected at 5 GHz, where the effect of Faraday rotation is largest, (ii) estimates of its properties may

be distorted by its proximity to the core, and (iii) we cannot exclude the possibility that it is optically thick at 8 GHz (see Fig. 6), which would have to be taken into account in a rotation-measure analysis. Unlike the core, I1, and S, the χ values for I2 do not show obvious evidence for a linear dependence on λ^2, and are consistent with a linear dependence only at about the 3σ level. At the same time, the nominal least-squares linear fit to these data yields a rotation measure that is plausible, and similar to that determined for I1:RM $= -104 \pm 26$. We will adopt this nominal rotation measure in our discussion below, but clearly this measurement is subject to considerable uncertainty, and must be treated as tentative.

4 DISCUSSION

4.1 The detected rotation-measure distribution

Our multifrequency VLBA observations indicate that the Faraday rotation occuring on parsec scales in 1803+784 is not uniform, with the rotation measure increasing toward the VLBI core. We would like to derive the 'intrinsic' rotation measures of the various regions in the VLBI structure – i.e. the rotation measures due to the contribution of thermal plasma in the immediate vicinity of the BL Lac object. To do this, we must determine the uniform foreground rotation measure due to the Galactic interstellar medium and subtract its contribution from the total observed rotation measure for each VLBI region.

The integrated rotation measure of 1803+784 derived from simultaneous VLA observations at multiple frequencies from 1.4–1.6 GHz is RM $= -61$ rad m^{-2} (Wrobel 1993; Pushkarev 2001). If the integrated polarization at these frequencies has an appreciable contribution from regions near the VLBI core, this value could be 'contaminated' by the effect of thermal plasma near the BL Lac object; if the integrated polarization primarily comes from regions further out in the VLBI jet, the integrated rotation measure should be a good estimate of the Galactic contribution.

We can try to estimate this constant Galactic contribution to the rotation measure by determining the rotation measure on parsec scales sufficiently far from the VLBI core that we no longer have any contribution from thermal plasma in the vicinity of the BL Lac object. We can see from Fig. 5 and Table 2 that polarization is detected beyond the stationary component S only at 5 GHz, making it impossible to use these four-frequency data to estimate the Galactic rotation measure.

This led us to consider the 1.6- and 5-GHz ground-array *P* images for our space-VLBI observations obtained on 1998 July 20 and 21 shown in Fig. 8. In both cases, polarization is detected far beyond S, extending out to $\simeq$30 mas from the core.

We estimated the 5- and 1.6-GHz χ values for 1998 July in two regions beyond component S, $\simeq$10 mas to the west of the core and $\simeq$30 mas to the southwest of the core (regions 1 and 2 marked in Fig. 8), by summing Q and U in these regions using the IMSTAT facility in AIPS. The resulting χ values for Region 1 are $\chi_5 = -19^\circ$ and $\chi_{1.6} = +78^\circ$; the χ values for Region 2 are $\chi_5 = -46^\circ$ and $\chi_{1.6} = -54^\circ$. The uncertainty for each is about 4° (based on the uncertainties in Q and U and an overall uncertainty in the absolute χ calibration at each frequency of 2–3°). In principle, the implied differences in χ are subject to $n\pi$ ambiguities, which we have no way to resolve, since we have measurements at only two frequencies. Allowing for the simplest case of an ambiguity of π in each of these measurements, the implied χ differences are $\Delta\chi_1 = -97^\circ \pm 6^\circ$ or $+83^\circ \pm 6^\circ$ for Region 1 and $\Delta\chi_2 = -100^\circ \pm 6^\circ$ or $+80^\circ \pm 6^\circ$ for Region 2. Accordingly, the implied rotation measures, are RM$_1$ $= -58 \pm 4$ rad m^{-2} or $+50 \pm 4$ rad m^{-2} for Region 1 and RM$_2$ $= -60 \pm 4$ rad m^{-2} or $+48 \pm 4$ rad m^{-2} for Region 2.

It is immediately apparent that the χ differences (and therefore rotation measures) for the two regions are the same within the errors. In addition, the negative rotation measure coincides with the integrated value, derived from VLA measurements at multiple frequencies from 1.4–1.6 GHz. In spite of the relatively large difference between the two wavelengths considered here and the uncertainty associated with possible $n\pi$ ambiguities, this provides strong evidence that the rotation measures in Region 1 and Region 2 are both Galactic; i.e. they are both due to the passage of the radiation through the interstellar medium of our Galaxy. This implies that the integrated rotation measure determined by Wrobel (1993) and later confirmed by Pushkarev (2001) provides an accurate estimate of the Galactic contribution, presumably because the polarization at the frequencies at which the integrated measurements were made (1.4–1.6 GHz) is dominated by emission from regions far enough from the VLBI core that there is a negligible contribution from thermal plasma near the active galactic nucleus (AGN).

Accordingly, we will subtract -61 rad m^{-2} from our measured rotation measures for the VLBI components C, I2, I1 and S to estimate the rotation measures corresponding to the thermal plasma in the immediate vicinity of the radio-emitting regions. In addition, to find the rotation measures in the rest frame of the source, we

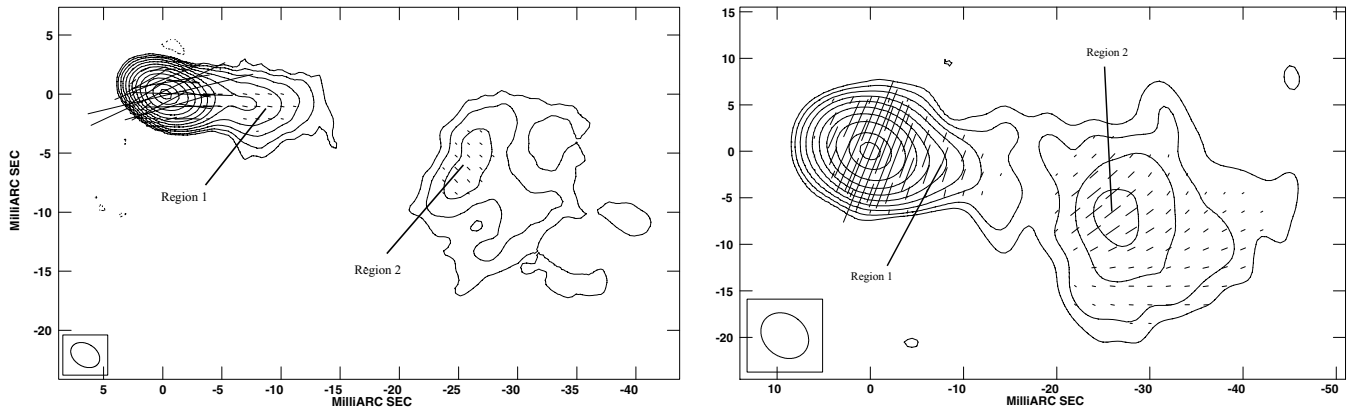

Figure 8. VLBI *I* maps of 1803+784 for epoch 1998.55 with χ sticks superimposed. Left: 5 GHz image with contours at -0.062, 0.062, 0.12, 0.25, 0.5, 1, 2, 4, 8, 16, 32 and 64 per cent of the peak brightness of 2.020 Jy beam^{-1}. Right: 1.6 GHz image with contours at -0.25, 0.25, 0.5, 1, 2, 4, 8, 16, 32 and 64 per cent of the peak brightness of 1.640 Jy beam^{-1}. The two regions for which we have estimated χ values are indicated.

Table 4. Component rotation measures.

	r (mas)	Observed RM rad m^{-2}	RM–RM$^{*}_{\rm Gal}$ rad m^{-2}	(RM–RM$_{\rm Gal}$)$^{\dagger}_{0}$ rad m^{-2}
C	–	-237 ± 6	-176 ± 6	-496 ± 20
I2	0.25	-104 ± 26	-43 ± 26	-121 ± 73
I1	0.60	-111 ± 13	-50 ± 13	-141 ± 37
S	1.50	-20 ± 15	$+41 \pm 15$	$+116 \pm 42$

*RM$_{\rm Gal} = -61$ rad m^{-2}. †After multiplication by $(1+z)^2$.

must multiply by a factor of $(1+z)^2 = 2.82$ for 1803+784; we will call the resulting quantity the 'intrinsic' rotation measure. We summarize the resulting values in Table 4. We can see that the intrinsic rotation measure is roughly -500 rad m^{-2} for the core, and decreases rapidly with distance from the core. The intrinsic rotation measure for I2 ($r \simeq 0.25$ mas) is equal to zero within the errors, while I1 ($r \simeq 0.6$ mas) may have a modest residual rotation measure after subtraction of the Galactic contribution. The close adherence to a λ^2 law for the core χ values (Fig. 7) and lack of depolarization at lower frequencies (Table 2) indicate that the thermal plasma associated with the Faraday rotation is external to the radio-emitting region.

The rotation measure for the stationary component S ($r \simeq 1.5$ mas) is formally consistent with zero at the 2.8σ level, but we cannot exclude the possibility that there is some modest *positive* rotation measure at this location. If the rotation measure of S is non-zero and positive, this would appear to reflect a change in the dominant orientation of the line-of-sight magnetic field at this location. It is an interesting possibility that this might somehow be related to the nature of this long-lived stationary feature (reflect a bend in the jet relative to the line of sight, for example), but at present this is only speculation.

4.2 Comparison of parsec-scale rotation measures estimated at different epochs

A preliminary joint analysis of our VSOP 1.6-GHz (1998 July 20) and ground-array 5-GHz (1998 July 21) images (Gabuzda 2000), which have comparable resolution, also suggested that regions near the core and the stationary component S might have different rotation measures. The derived rotation measures are subject to $n\pi$ ambiguities, which we cannot resolve in the absence of additional information, since we have measurements at only two (widely-spaced) frequencies. For the two frequencies observed, this corresponds to ambiguities of $\pm 110n$ rad m^{-2} in the rotation measure. In the simplest case of an ambiguity of π in the χ measurements, the implied rotation measures were about $+25$ or -85 rad m^{-2} for the core region and $+60$ or -50 rad m^{-2} for the vicinity of S. One alternative value for the core would be $-85 - 110 = -195$ rad m^{-2}, similar to the core value reported here (-237 rad m^{-2}). In the case of S, the value -50 rad m^{-2} is consistent with the 1997 April value (-20 rad m^{-2}) to within 1–2σ. If these do represent independent measurements of the same value, it is difficult to be sure which is more accurate: the 1997 April estimate is based on measurements at more than two frequencies, but the lower-frequency 1998 July estimate is more sensitive to small rotation measures.

Additional multifrequency, multi-epoch VLBA polarization observations currently being reduced should enable us to confirm the general behaviour displayed by our 1997 April measurement and also test for time variability of the parsec-scale rotation-measure distribution in 1803+784.

4.3 Properties of the thermal gas and the region in which it is located

It is of interest to try to use the derived intrinsic rotation measures to infer information about the electron density and magnetic field in the region of thermal plasma giving rise to the Faraday rotation near the VLBI core. Unfortunately, this is complicated by the fact that the rotation measure depends on both of these quantities, as well as the line-of-sight pathlength of the polarized radiation through the region of thermal plasma, and we have no way to unambiguously disentangle the contributions of these three quantities. However, we can make a rough consistency check as follows.

The definition of the rotation measure is (Burn 1966; Tucker 1975)

$$\mathrm{RM} = 8.1 \times 10^5 \int N_{\rm e} \boldsymbol{B} \cdot \mathrm{d}\boldsymbol{l},$$

which can be approximated

$$\mathrm{RM} \simeq 8.1 \times 10^5 N_{\rm e} B_{\parallel} L \qquad (1)$$

in the case of electromagnetic radiation travelling a length L through a region of roughly homogeneous thermal plasma with the magnetic-field component along the line of sight equal to $B_{\parallel}$. Here, L is in pc, B and $B_{\parallel}$ are in G, the electron number density $N_{\rm e}$ is in cm^{-3}, and RM is in rad m^{-2}. If we further assume that this Faraday-rotating gas is in equipartition, we have the additional relation

$$N_{\rm e} kT \simeq \frac{B^2}{8\pi} \qquad (2)$$

Eliminating $N_{\rm e}$ and multiplying the observed rotation measure by $(1+z)^2$ to determine the RM in the source frame, we obtain

$$B^2 B_{\parallel} \simeq \frac{\mathrm{RM}(1+z)^2 \pi k T}{10^5 L}.$$

Approximating $B_{\parallel} \simeq B$, as we expect if the magnetic field has no special orientation relative to the line of sight to the radio source (this approximation should affect the final result by at most about a factor of two or so),

$$B^3 \simeq \frac{\mathrm{RM}(1+z)^2 \pi k T}{10^5 L}$$

$$B \simeq \left[\frac{\mathrm{RM}(1+z)^2 \pi k T}{10^5 L}\right]^{1/3}. \qquad (3)$$

Now let us suppose that this gas has properties fairly typical of narrow-line clouds. In particular, let us assume that its temperature is $T \simeq 10^4$ K, as has been established from observations of forbidden and semi-forbidden lines (Koski 1978; Heckman & Balick 1979). Substituting this value together with the observed RM for the VLBI core, the redshift of 1803+784, and the Boltzmann constant, we obtain

$$B \simeq 27.8 L^{-1/3}. \qquad (4)$$

where B is now in μG. Further, substituting RM$(1+z)^2$ together with this expression for B into (1), we find for the corresponding electron density in cm^{-3}

$$N_{\rm e} \simeq 22.0 L^{-2/3}. \qquad (5)$$

Thus, we can get at least rough estimates of B and $N_{\rm e}$ if we can put limits on the extent of the region of thermal gas giving rise to the rotation measure. Since the intrinsic RM of I2 ($r \simeq 0.25$ mas) is consistent with zero within the errors and the nominal intrinsic RM of I1 ($r \simeq 0.6$ mas) is modest at best (less than one-third the

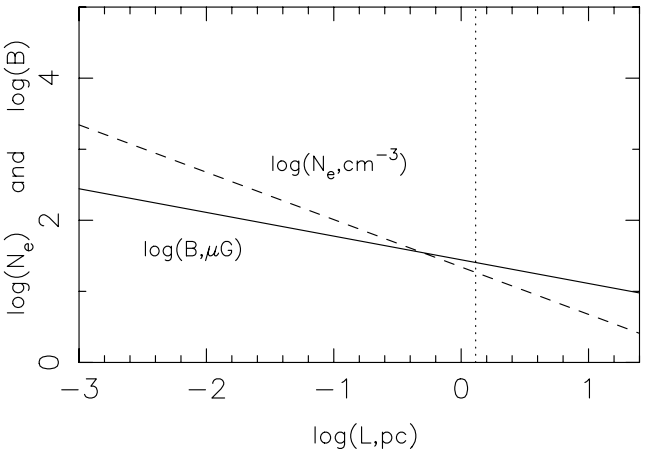

Figure 9. Estimated dependence of the electron density N_e (dashed line) and magnetic field B (solid line) in the region of enhanced Faraday rotation near the VLBI core on the pathlength through this region L. These dependences assume that the associated thermal gas is in equipartition and that the distribution of the gas is roughly uniform. The dotted vertical line shows our estimated upper limit for the extent of the region occupied by the thermal gas, so that the inferred N_e and B values lie to the left of this line.

core value), we will take the size of the region of thermal gas in the plane of the sky to be $\leqslant$0.25 mas. Since 1 mas = 5.27 pc at the redshift of 1803+784, this implies a size $L \leqslant 1.3$ pc, if the extent of this region along the line of sight is roughly equal to its extent in the plane of the sky. Substituting this value into expressions (4) and (5), we obtain $B \geqslant 25$ μG and $N_e \geqslant 18$ cm^{-3}.

Relations (4) and (5) are shown in the log–log plots in Fig. 9. The vertical dotted line corresponds to the indicated crude upper limit for the extent of the region of thermal plasma, $L = 1.3$ pc. These plots demonstrate the increase in the inferred values for B and N_e as L decreases. If the intrinsic rotation measure in the vicinity of the core has, in fact, already reached zero by the position of I2, the extent of the region of thermal gas is probably a factor of a few or more smaller than indicated above. If this size is $L \simeq 0.3$ pc, the corresponding magnetic field and electron density are $B \simeq 40$ μG, which seems plausible given inferred ***B*** fields on kiloparsec scales ($\simeq$0.15–1.5 μG; see for example, Laing & Bridle 1987), and $N_e \simeq 50$ cm^{-3}, roughly consistent with the expected electron densities in narrow-line clouds ($\sim 10^2$–10^4 cm^{-3}).

While this analysis does not provide firm estimates, it does suggest that the parameters of the thermal gas associated with the enhanced Faraday rotation in the vicinity of the VLBI core are consistent with current concepts about gas that may be present on parsec scales, e.g. in narrow-line clouds. 1803+784 is now the second BL Lac object to our knowledge that has been found to exhibit enhanced Faraday rotation in the vicinity of its VLBI core, the other being BL Lac itself (Reynolds et al. 2001), for which the intrinsic VLBI core rotation measure was found to be RM $\simeq -430$ rad m^{-2}. In addition, a region of enhanced rotation measure well separated from the VLBI core with intrinsic rotation measure RM $\simeq +1340$ rad m^{-2} has been observed in 0820+225 (Gabuzda, Pushkarev & Garnich 2001).

Although lower than the values derived for a number of quasars that have intrinsic core rotation measures in excess of 2000 rad m^{-2} (Taylor 1998, 2000), the core rotation measures of 1803+784 and BL Lac are comparable to or even higher than values for several other quasars in the same sample (3C 395, 800 rad m^{-2}; 2230+114, 660 rad m^{-2}; 3C 345, 330 rad m^{-2}; Taylor 1998, 2000). Thus, the core rotation measures provide no compelling evidence for a dearth of thermal gas in the BL Lac objects. Since these three quasars have appreciably more luminous optical emission lines than the two BL Lac objects, this suggests that the relative weakness of the optical lines in the BL Lac objects is due to some other factor, such as a lower-luminosity ionizing continuum.

4.4 Evidence for a helical jet magnetic field in 1803+784

Previous VLBI polarization observations of 1803+784 (Gabuzda et al. 1992, 1994; Gabuzda & Cawthorne 1996; Gabuzda 1999) have shown the dominant jet ***B*** field on scales out to several mas from the core to be transverse to the jet direction. There is firm evidence that the intrinsic electric vector χ in the core is usually aligned with the direction of the inner jet. At first, it seems that this is not the case in our 1997 April images, since the first knot detected in the jet lies in position angle $\theta = -87^\circ$, while the zero-wavelength χ for the core is about -40°. However, some earlier images have shown the presence of motion very near the core in position angle $\simeq -(45$–$60)^\circ$ (Gabuzda & Cawthorne 1996; Gabuzda 1999). Thus, it seems likely that the intrinsic orientation of the core χ in our 1997 April images reflects the direction of the jet flow on scales somewhat smaller than our resolution. It is not clear whether the initial direction of the jet flow is always about -45°, after which the jet turns toward the west, or if the direction in which new jet components emerge varies over some range of position angles, although there is some evidence for the latter from mm-VLBI observations (e.g. Krichbaum et al. 1993).

The intrinsic polarization position angles χ_0 for more extended regions further from the core can be determined by correcting them for the Galactic rotation measure. Since these regions are optically thin, the inferred ***B*** field will then be perpendicular to χ_0 (see discussion in the Introduction). Fig. 10 shows the 5-GHz VLBI I map of 1803+784 from Fig. 8 with these ***B*** vectors superposed. We can clearly see that the inferred ***B*** field in the extended regions of emission at 5 GHz is transverse to the jet direction. At the same time, the results for the corresponding full-resolution 5-GHz space-VLBI images (Gabuzda 1999) demonstrate that the jet is appreciably curved on scales out to $\simeq$2 mas from the core, and that the ***B*** field in this inner jet is likewise everywhere transverse to the jet direction. Thus, the dominant ***B*** field in the jet of 1803+784 is perpendicular to the jet direction on all observed scales from 0–30 mas, or a distance projected on to the plane of the sky of roughly 0–150 pc at the redshift of 1803+784. This argues in favour of the idea initially proposed by Gabuzda (1999) that we are detecting the dominant toroidal

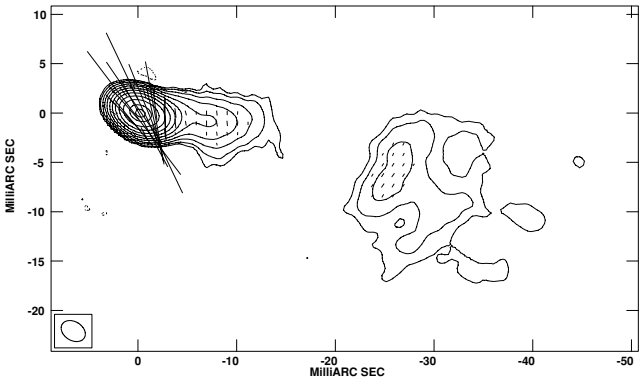

Figure 10. 5-GHz VLBI I map of 1803+784 from Fig. 8 with ***B*** vectors superposed.

component of a helical field associated with the VLBI jet: this picture can provide a natural explanation for the fact that the dominant jet ***B*** field is everywhere transverse, independent of whether a section of the jet flow is curved/straight or compact/extended.

5 CONCLUSION

We have presented new VLBI *I* and *P* images at 5, 8, 15 and 22 GHz for 1997 April 6, and at 1.6 and 5 GHz for 1998 July 20 and 21, concentrating on analysis of the four-frequency images; a more complete analysis of the 1998 July images will be presented in a future paper.

(i) We were able to derive spectral information for four features detected at 3–4 frequencies: the core and three components in the inner jet. The spectrum of the core is very flat from 5–22 GHz. A feature at $r \simeq 0.25$ mas, which is resolved from the core only above 5 GHz, has an inverted spectrum, suggesting it is either optically thick below about 15 GHz or subject to low-frequency absorption. The spectral index for another jet feature $\simeq$0.6 mas from the core is between -0.7 and -2 between 5 and 15 GHz, as expected if it is optically thin. The spectral index flattens at a component about 1.5 mas from the core, possibly suggestive of particle reacceleration that may be related to the nature of this long-lived, nearly stationary feature.

(ii) The core polarization is modest and comparable at all frequencies ($\simeq$3.5 per cent). The various jet components are polarized $\simeq$4–16 per cent, as is quite typical of compact radio-loud AGN.

(iii) Comparison of the 1997 April polarization images and model-fitting results for the different frequencies revealed a gradient in the rotation-measure distribution on parsec scales, with an enhancement of the rotation measure in the VLBI core. Non-uniformity in the rotation measure on such small scales must be due to inhomogeneity in the properties of the medium in the immediate vicinity of the radio-emitting region. The close adherence to a λ^2 law for the core χ values (Fig. 7) and lack of depolarization (Table 2) indicate that the thermal plasma associated with the Faraday rotation is external to the radio-emitting region.

(iv) An analysis of the polarization properties of emission $\simeq$10–30 mas from the core in our deep 1.6- and 5-GHz *P* images for 1998 July confirms that the Galactic contribution to the observed rotation measures is accurately described by the previously published value of -61 rad m^{-2} (Wrobel 1993; Pushkarev 2001).

(v) Previous observations have consistently shown that the dominant jet ***B*** field within several mas of the core is typically transverse to the jet direction, as is also the case for the images presented here. Our 1998 July *P* images corrected for the Galactic rotation measure demonstrate that the jet ***B*** field structure remains transverse at least to $\simeq$30 mas from the core. This supports the view that we are detecting the dominant toroidal component of a helical ***B*** field associated with the jet (Gabuzda 1999).

(vi) Subtracting the Galactic contribution to the total rotation measure from the observed VLBI core rotation measure and multiplying by $(1 + z)^2$ yields an 'intrinsic' rotation measure in the rest frame of the source of -496 ± 20 rad m^{-2}. Non-uniform parsec-scale rotation-measure distributions have now been detected in at least three BL Lac objects: BL Lac (Reynolds et al. 2001), 0820+225 (Gabuzda et al. 2001), and 1803+784 (this paper). The magnitudes of the corresponding source rest-frame rotation measures vary from about 400 to 1300 rad m^{-2}, within the range of values measured for a sample of quasars with appreciably more luminous optical line emission (Taylor 1998, 2000). This makes it unlikely that the weak optical line emission characteristic of BL Lac objects reflects a dearth of thermal gas. BL Lac objects do not appear to be systematically more beamed than core-dominated quasars (Ghisellini et al. 1993), and the emission lines of BL Lac objects are intrinsically of low luminosity compared to the typical line luminosities of quasars (Padovani 1992). Thus, it is also not the case that the emission lines of BL Lac objects are intrinsically strong but 'swamped' by a highly-beamed optical continuum. The most simple and plausible explanation for the weakness of the optical emission lines of BL Lac objects may be that the ionizing continuum radiation is insufficient to produce optical lines as luminous as those in quasars.

Since it is likely that FR I radio galaxies represent the parent population of most BL Lac objects (Browne 1983; Wardle, Moore & Angel 1984), this is also consistent with the analysis of Baum, Zirbel & O'Dea (1995), who found the optical emission lines of FR I radio galaxies to be systematically less luminous than those of FR II radio galaxies of the same total radio luminosity or radio core power, and concluded that this was probably associated with a lack of ionizing uv continuum in FR I sources, rather than a lack of thermal gas.

ACKNOWLEDGMENTS

We would like to thank Cormac Reynolds for work on the preliminary calibration of the 1997 April data and useful discussions during our preparation of the manuscript. DCG acknowledges support from the European Commission under the IHP Programme (ARI) contract No. HPRI-CT-1999-00045. The National Radio Astronomy Observatory is operated by Associated Universities, Inc., under cooperative agreement with the NSF. We gratefully acknowledge the VSOP Project, which is led by the Japanese Institute of Space and Astronautical Science in cooperation with many organizations and radio telescopes around the world.

REFERENCES

Baum S. A., Zirbel E. L., O'Dea C. P., 1995, ApJ, 451, 88
Blandford R. D., 2003, in Circular Polarization from Relativistic Jet Sources. In press
Britzen S., Witzel A., Krichbaum T. P., Muxlow T. W. B., 1999, New Astron. Rev., 43, 751
Browne I. W. A., 1983, MNRAS, 204, 23P
Burn B. J., 1966, MNRAS, 133, 67
Gabuzda D. C., 1999, New Astron. Rev., 43, 691
Gabuzda D. C., 2000, in Astrophysical Phenomena Revealed by Space VLBI. ISAS, Tokyo, p. 121
Gabuzda D. C., Cawthorne T. V., 1996, MNRAS, 283, 759
Gabuzda D. C., Wardle J. F. C., Roberts D. H., 1989, ApJ, 338, 743
Gabuzda D. C., Cawthorne T. V., Roberts D. H., Wardle J. F. C., 1992, ApJ, 388, 40
Gabuzda D. C., Mullan C. M., Cawthorne T. V., Wardle J. F. C., Roberts D. H., 1994, ApJ, 435, 140
Gabuzda D. C., Pushkarev A. B., 2001, 327, 1
Ghisellini G., Padovani P., Celotti A., Maraschi L., 1993, ApJ, 407, 65
Heckman T. M., Balick B., 1979, A&A, 79, 350
Hirabayashi H. et al., 1998, Sci., 281, 1825
Istomin Y. N., Pariev V. I., 1994, MNRAS, 267, 629
Kollgaard R. I., Wardle J. F. C., Roberts D. H., Gabuzda D. C., 1992, AJ, 104, 1687
Koski A. T., 1978, ApJ, 223, 56
Krichbaum T. P., Witzel A., Graham D. A., Schalinski C. J., Zensus J. A., 1993, in Davis R. J., Booth R. S., eds, Subarcsecond Radio Astronomy. Cambridge Univ. Press, Cambridge, p. 181

Laing R. A., Bridle A. H., 1987, MNRAS, 228, 557
Lawrence C. R., Readhead A. C. S., Pearson T. J., Unwin S. C., 1987, in Superluminal Radio Sources. Cambridge Univ. Press, Cambridge, p. 260
Padovani P., 1992, MNRAS, 257, 404
Pushkarev A. B., 2001, Astron. Rep., 45(9), 667
Reynolds C., Cawthorne T. V., Gabuzda D. C., 2001, MNRAS, 327, 1071
Roberts D. H., Wardle J. F. C., Brown L. F., 1994, ApJ, 427, 718
Schalinski C. J., Alef W., Witzel A., Campbell J., Schuh H., 1988, in Reid M. H., Moran J. M., eds, The Impact of VLBI on Astrophysics and Geophysics. Kluwer, Dordrecht, p. 359
Strom R. G., Biermann P. L., 1991, A&A, 242, 313
Taylor G. B., 1998, ApJ p. 506, 637
Taylor G. B., 2000, ApJ, 533, 95
Tucker W. H., 1975, Radiation Processes in Astrophysics. Massachusetts Institute of Technology, Cambridge, MA, p. 50
Wardle J. F. C., Moore R. L., Angel J. R. P., 1984, ApJ, 279, 93
Witzel A., Schalinski C. J., Johnston K. J., Biermann P. L., Krichbaum T. P., Hummel C. A., Eckart A., 1988, A&A, 206, 245
Wrobel J., 1993, AJ, 106, 444

This paper has been typeset from a TEX/LATEX file prepared by the author.